

Hydrogen Maser Frequency Standard Computer Model for Automatic Cavity Tuning Servo Simulations

P. D. Potter and C. Finnie
Radio Frequency and Microwave Subsystems Section

A computer model of the JPL hydrogen maser frequency standard has been developed. This model allows frequency stability data to be generated, as a function of various maser parameters, many orders of magnitude faster than these data can be obtained by experimental test. In particular, the maser performance as a function of the various automatic tuning servo parameters may be readily determined.

I. Introduction

Hydrogen maser frequency standards generally display frequency stability characteristics which are strong functions of the observation period over which the stability is measured. As long-term (hours to weeks) stability is of great interest in DSN tracking, testing periods for hydrogen masers are lengthy. In some cases a computer simulation may expeditiously provide performance data which would be impractical to obtain experimentally.

A convenient and widely accepted characterization of frequency stability is the Allan Variance Chart (Ref. 1). Given a frequency standard whose output voltage $V(t)$ may be expressed as

$$V(t) = [V_0 + \epsilon(t)] \sin [2\pi\nu_0 t + \phi(t)] \quad (1)$$

The fractional instantaneous frequency deviation $y(t)$ may be defined as

$$y(t) \equiv \left(\frac{1}{2\pi\nu_0} \right) \frac{d\phi(t)}{dt} \quad (2)$$

The k th average value of $y(t)$, \bar{y}_k , over a time interval of length τ is given by

$$\bar{y}_k = \frac{1}{\tau} \int_{t_k}^{t_k + \tau} y(t) dt \quad (3)$$

The Allan variance $\sigma_y^2(\tau)$ is defined as

$$\sigma_y^2(\tau) \equiv \left\langle \frac{(\bar{y}_{k+1} - \bar{y}_k)^2}{2} \right\rangle \quad (4)$$

where $\langle \rangle$ denotes an infinite time average. In practice $\sigma_y^2(\tau)$ is estimated as

$$\sigma_y^2(\tau) \approx \frac{1}{m} \sum_{k=1}^m \frac{(\bar{y}_{k+1} - \bar{y}_k)^2}{2} \quad (5)$$

In this article a hydrogen maser computer model is described which generates the $y(t)$ and $\sigma_y^2(\tau)$ corresponding to the selected values of noise sources and the autotuner (if used) parameters.

II. The Hydrogen Maser Autotuner Servo

The maser cavity autotuner system has been previously described (Refs. 2, 3, 4). The purpose of the autotuner is to electronically bring the cavity resonant frequency f_c into alignment with the atomic hydrogen transition frequency f_n . The effect of cavity pulling on the maser output frequency f_0 is given by (Ref. 2)

$$f_n - f_0 \approx (f_n - f_c) \frac{Q_c}{Q_L} \quad (6)$$

where

$$Q_c = \text{loaded cavity quality factor } (\approx 3.5 \times 10^4)$$

$$Q_L = \text{atomic hydrogen transition quality factor } (\approx 10^9)$$

The basic principle of operation of the autotuner is to periodically change Q_L and to electronically adjust f_c until the change of Q_L does not affect f_0 . In this way changes in the maser output frequency f_0 due to mechanical changes in the cavity may be eliminated.

Figure 1 (from Ref. 4) shows the block diagram of the cavity tuning servo system. The atomic quality factor Q_L is varied by an atomic hydrogen beam flux chopper. Variations in the maser output frequency relative to a reference frequency standard are measured by the zero crossing detector and are used to generate a correction voltage on a varactor in the cavity output circuit. The maser fractional frequency deviation $\Delta f/f_0$ is related to the time deviation $\Delta\tau$ in the zero crossing detector by

$$\frac{\Delta f}{f_0} = \left(\frac{\Delta\tau}{\tau_0^2} \right) \left(\frac{1}{f_0} \right) \quad (7)$$

where

$$\tau_0 = \text{nominal beat period} = 100 \text{ s}$$

$$f_0 = \text{frequency} = 100 \text{ MHz}$$

Thus, for example, a beat period change of 0.1 s corresponds to a fractional frequency variation of 10^{-13} .

Figure 2 (from Ref. 4) shows the method used to develop the cavity tuning error signal. In the period τ_1 the up count is during a time of high beam flux, and during the period τ_3 the down count is during a period of low flux. During the τ_5 and τ_7 periods the up-down count has a reversed relationship to the flux level. By subtracting these two up-down

counts, a first-order correction is made for frequency shifts which are not caused by the flux level modulation.

Figure 3 (from Ref. 3) is the autotuner servo diagram, where the four-position switches schematically represent the four counting periods shown in Fig. 2. The summing counter is a perfect integrator, resulting in a first-order servo loop with the only adjustable parameter being the loop gain factor K_s . Performance of this servo loop and also possible second-order loop designs are discussed in Sections V and VI below.

III. Hydrogen Maser Computer Model Noise Sources

The computer model operates as a sampled-data system in the same fashion as experimental setups, except the sampling rate is many orders of magnitude greater than with the experimental system, thus allowing for expeditious evaluation of the effects of maser parameters upon the Allan Variance Chart.

Four different types of noise are presently available in the computer model: (1) oscillator shot noise, (2) flicker noise, (3) linear drift and (4) sinusoidally varying drift. Each of these types of noise has a characteristic slope relationship to the averaging period τ on an Allan Variance Chart (Ref. 1). For the oscillator shot noise, the square root of the Allan variance $\sigma(\tau)$ decays as $1/\tau^{1/2}$ and is typically only significant for τ values less than approximately 10^3 s. The theoretical value for this type of noise for the JPL maser is (Ref. 5)

$$\sigma_y(\tau) = \left[\left(\frac{Q_c}{Q_e} \right) \left(\frac{S_0}{2P_s Q_L^2} \right) \left(\frac{1}{\tau} \right) \right]^{1/2} \approx \frac{2.3 \times 10^{-14}}{\tau^{1/2}} \quad (8)$$

where

$$Q_c = \text{loaded cavity } Q \approx 3.5 \times 10^4$$

$$Q_e = \text{external cavity } Q \approx 9.6 \times 10^4$$

$$Q_L = \text{hydrogen line } Q \approx 10^9$$

$$S_0 = \text{thermal power spectral density} \approx 4.4 \times 10^{-21} \text{ W/Hz}$$

$$P_s = \text{cavity power output} \approx 1.5 \times 10^{-12} \text{ W}$$

This type of noise has a flat frequency spectrum and is obtained in the computer model from a pseudorandom number generator.

The flicker noise has no theoretical basis. This type of

noise has a $1/f$ spectral density and results in an Allan variance which is independent of τ . An algorithm for generating this type of noise with a computer has been published (Ref. 6); however, the required computer time for this algorithm is proportional to the square of the number of data points, resulting in unreasonable execution times. The method used in the computer model described here is as follows. A set of 2^M data points is obtained from a pseudorandom number generator and then transformed to the frequency domain by a fast Fourier transform (FFT). The resulting spectral components are multiplied by a $1/f^{1/2}$ factor and inverse-transformed to the time domain. The time required for N data points is approximately proportional to $N \log N$ for this algorithm. Figure 4 shows an Allan Variance Chart for flicker noise generated by this algorithm; also shown are the 1-sigma error bars for the square root of the Allan variance.

The linear drift noise is characteristic of aging and/or mechanical creep in the maser cavity and has a characteristic slope of unity on the Allan Variance Chart. The sinusoidal noise typically results from diurnal variations in the temperature and barometric pressure environment of the maser. Figure 5 is an Allan Variance Chart of computed performance for typical values of shot noise, flicker noise and diurnal noise.

IV. Autotuner Computer Model

The autotuner is a sampled-data servo loop (Ref. 7) which performs the operations shown in Figs. 2 and 3. For such systems the signal exists only at discrete times, separated by the switching interval τ . The S-plane response of such systems is repetitive at frequencies of $\omega = \pm 2\pi n/\tau$. For purposes of analysis it is convenient to use the Z-transform, defined by

$$Z \equiv e^{T_s} = e^{\alpha\tau} e^{j\omega\tau} \quad (9)$$

Using this transform, the central S-plane strip defined by $-(\pi/\tau) \leq \omega \leq (\pi/\tau)$, $-\infty \leq \alpha \leq 0$ is mapped into a unit circle in the Z-plane. The other repetitive strips of the left half of the S-plane are mapped into this same unit circle in the Z-plane.

A general second-order sampled-data servo loop is shown in Fig. 6. A first-order loop such as the existing autotuner is a special case with $K_3 = K_2 = 0$. Figure 6 is easily implemented in the computer model with each of the "τ" boxes representing a storage register. Figure 7 is a simplified flowchart for the hydrogen maser computer model including the autotuner servo.

V. First-Order Autotuner Loop

For the existing autotuner with a first-order loop, the loop gain is the only servo parameter which is available for optimization. Presently available values for loop gain with the JPL maser nominal 10% line Q modulation (a ratio of 0.9) are approximately 0.001, 0.01 and 0.1; these correspond to autotuner noise gain settings of 0.01, 0.1 and 1 respectively. Figure 8 shows the computer model responses to step inputs of 10^{-12} , for noise gain settings of 0.1 and 1.0. In normal usage the 0.1 setting is used to prevent excessive noise on the varactor as shown in Fig. 8. The response time for this setting is approximately 10 hours, which is too slow for control of diurnal effects.

Figure 9 shows the computer model Allan Variance Chart for a noise gain setting of 1.0 and various flux modulation ratios and illustrates the effect of beam modulation noise. Also shown in Fig. 9 is a set of experimental data, confirming the high noise level associated with the 1.0 gain setting. Figure 10 shows a comparison of computed and measured data for the normally used noise gain setting of 0.1. Figure 11 shows the expected autotuner response for various values of the Q ratio. The improved performance for increased Q modulation is clearly evident. This parameter is fixed by the maser cavity coupling design, however; substantial redesign would be necessary to reduce the Q ratio to 0.4 - 0.6.

VI. Second-Order Autotuner Loop

Using the computer model, a second-order autotuner loop was investigated. With reference to Fig. 6, the closed loop response, $H(Z)$ may be expressed as

$$H(Z) = \frac{K_1(Z - K_3)}{(Z - Z_1)(Z - Z_2)} \quad (10)$$

where

$$Z_1, Z_2 = \frac{1 + K_2 - K_1}{2} \pm j \frac{\sqrt{4(K_2 - K_1 K_3) - (1 + K_2 - K_1)^2}}{2} \quad (11)$$

$$\equiv e^{-\omega_0\tau \cos \alpha} e^{\pm j\omega_0\tau \sin \alpha}$$

$\cos \alpha =$ loop damping

$\omega_0 \tau \sin \alpha = \omega_n =$ loop natural frequency

With the second-order loop, the natural frequency (bandwidth) and the damping may be independently selected. Figure 12 shows the loop response as a function of damping for a loop natural frequency of 8.7×10^{-5} rad/s (20-h time constant); a damping value of 0.707 ($1/\sqrt{2}$) critical is optimal, a result generally obtained in servo design. Figure 13 shows the performance as a function of loop time constant for the

optimal 0.707 critical damping; a time constant value of approximately 20 h appears optimal.

VII. Comparison of Second- and First-Order Loops

Figure 14 shows a comparison of optimal second- and first-order loops, for 10% Q modulation. It is concluded from this study that for the present JPL maser parameter values, the additional complexity of a second-order loop is not warranted.

References

1. Barnes, J. A., et al., "Characterization of Frequency Stability," NBS Technical Note 394, October 1970.
2. Finnie, C., "Frequency Generation and Control: Atomic Hydrogen Maser Frequency Standard," in *The Deep Space Network*, Technical Report 32-1526, Vol. I, Jet Propulsion Laboratory, Pasadena, Calif., pp 73-75.
3. Finnie, C., "Design of Hydrogen Maser Cavity Tuning Servo," in *The Deep Space Network*, Technical Report 32-1526, Vol. II, Jet Propulsion Laboratory, Pasadena, Calif., pp 86-88.
4. Finnie, C., "Tracking and Ground-Based Navigation: Hydrogen Maser Frequency Standard Automatic Cavity Tuning Servo," in *The Deep Space Network*, Technical Report 32-1526, Vol. XIV, Jet Propulsion Laboratory, Pasadena, Calif., pp 56-59.
5. Cutler, L. S., and Searle, C. L., "Some Aspects of the Theory and Measurement of Frequency Fluctuations in Frequency Standards," *Proc. IEEE*, Vol. 54, No. 2, Feb. 1966, pp 136-154.
6. Barnes, J. A., and Allan, D. W., "A Statistical Model of Flicker Noise," *Proc. IEEE*, Vol. 54, No. 2, Feb., 1966, pp 176-178.
7. Jury, E. I., *Sampled-Data Control Systems*, John Wiley and Sons, Inc., New York, 1958.

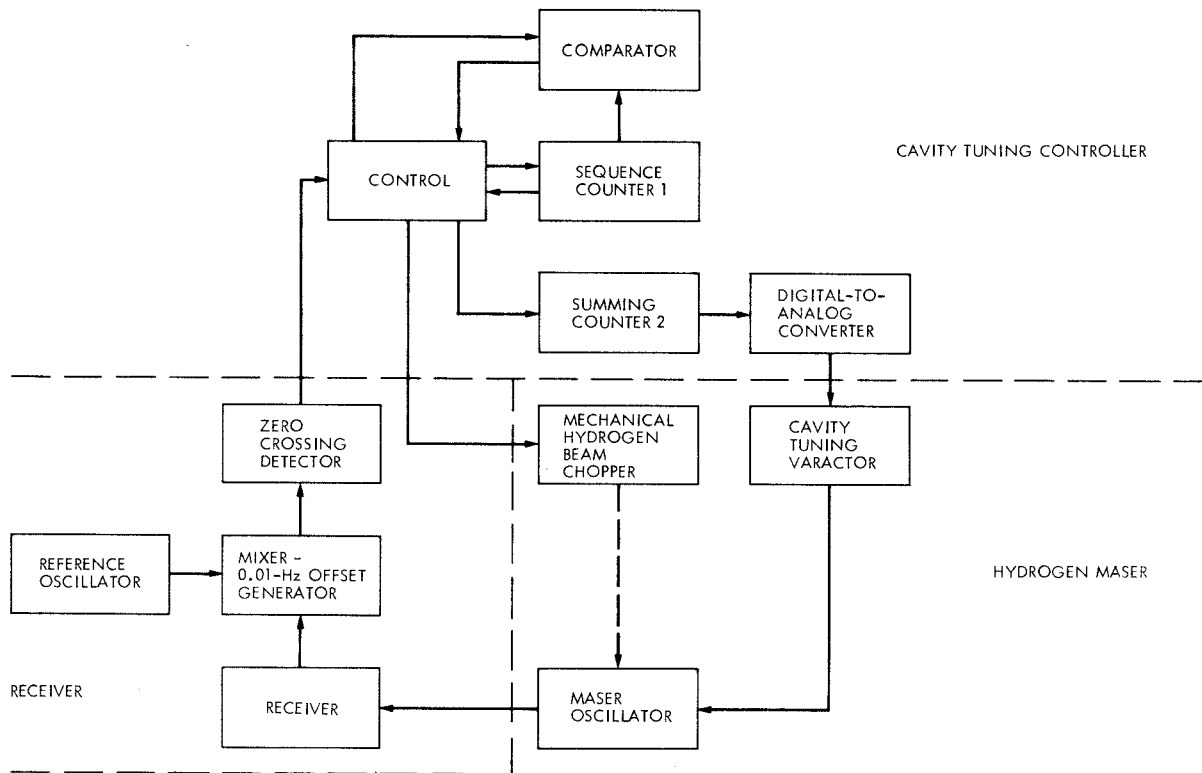


Fig. 1. Cavity tuning servo system block diagram

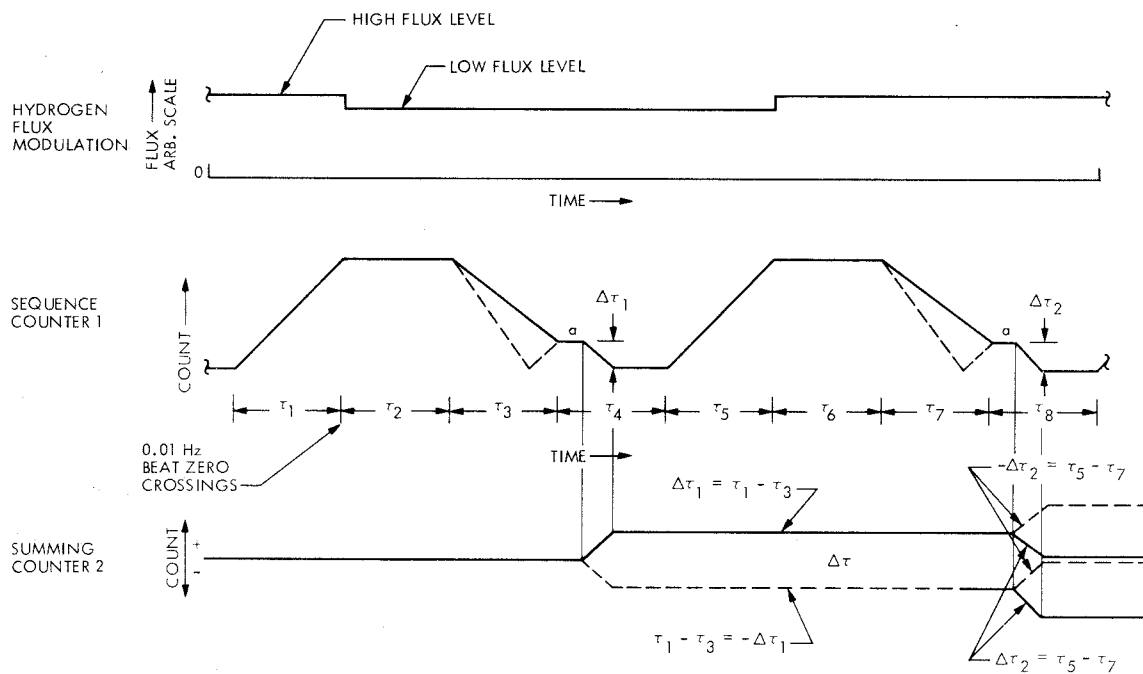


Fig. 2. Tuning mode count sequence diagram

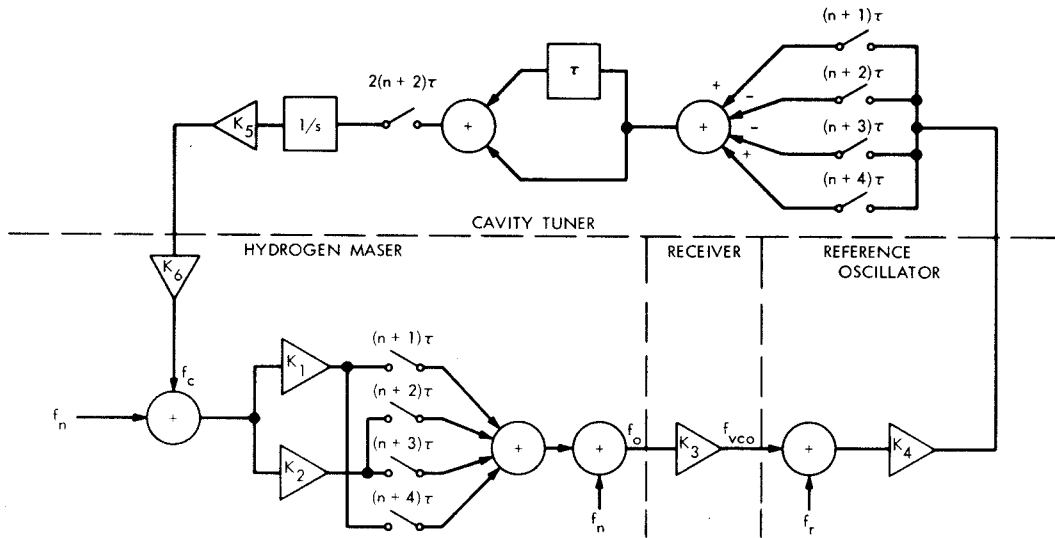


Fig. 3. Cavity tuner servo diagram

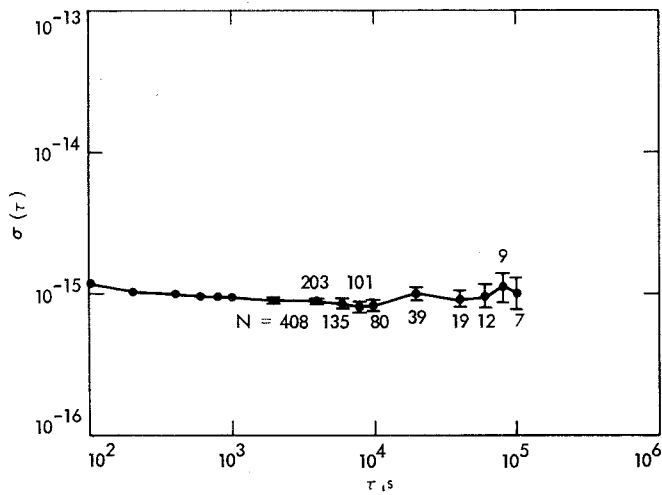


Fig. 4. Flicker noise generator performance

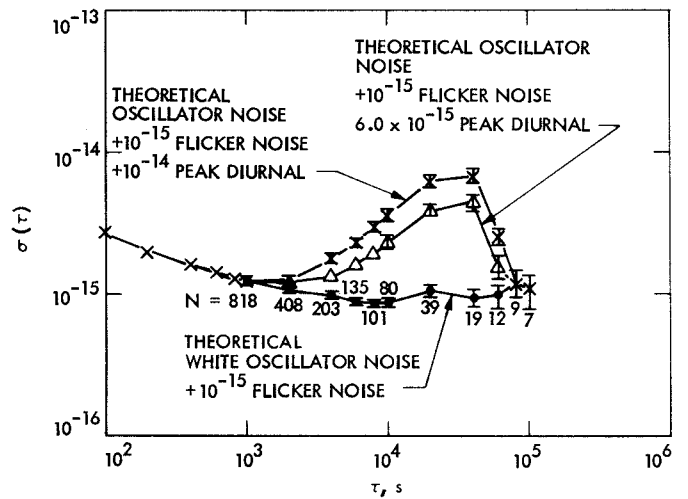


Fig. 5. JPL hydrogen maser computer simulations, no autotuning

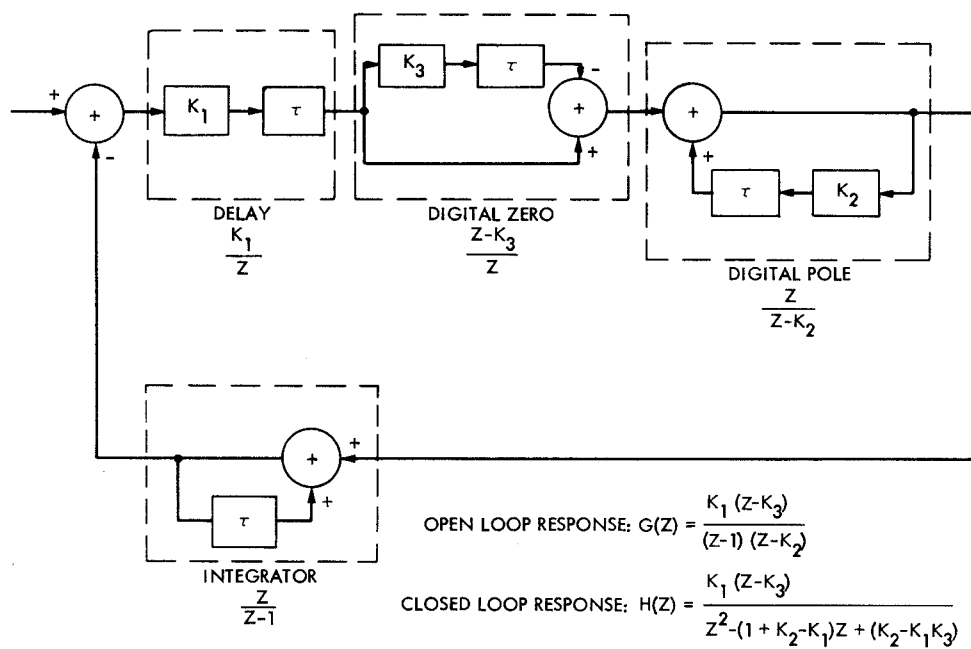


Fig. 6. Second-order sampled data servo loop

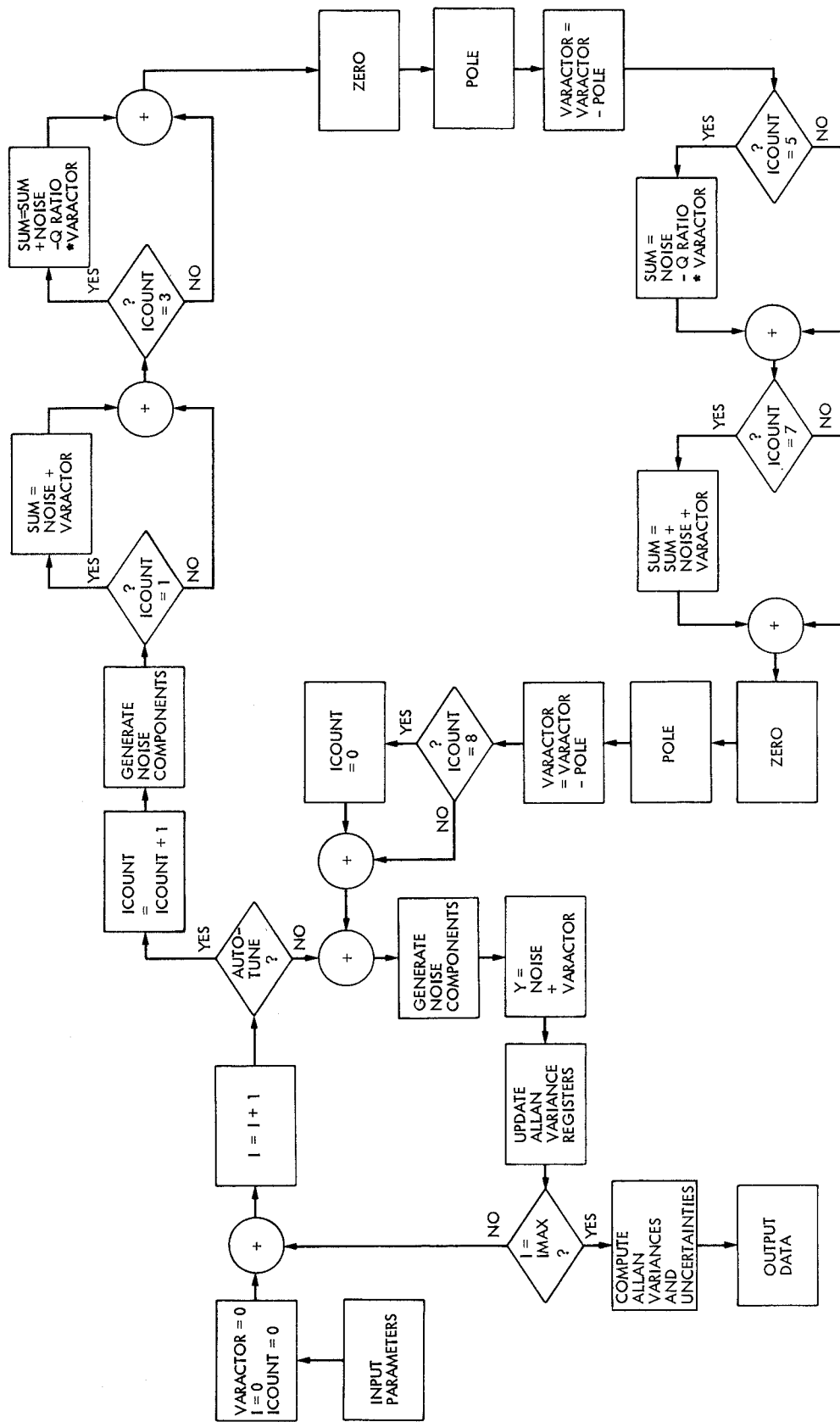


Fig. 7. Simplified hydrogen maser computer model flow chart

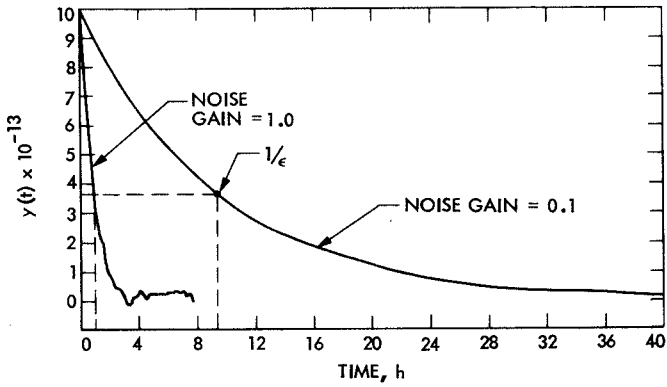


Fig. 8. Computer simulation of autotuner response to a 10^{-12} step input, .90 Q ratio

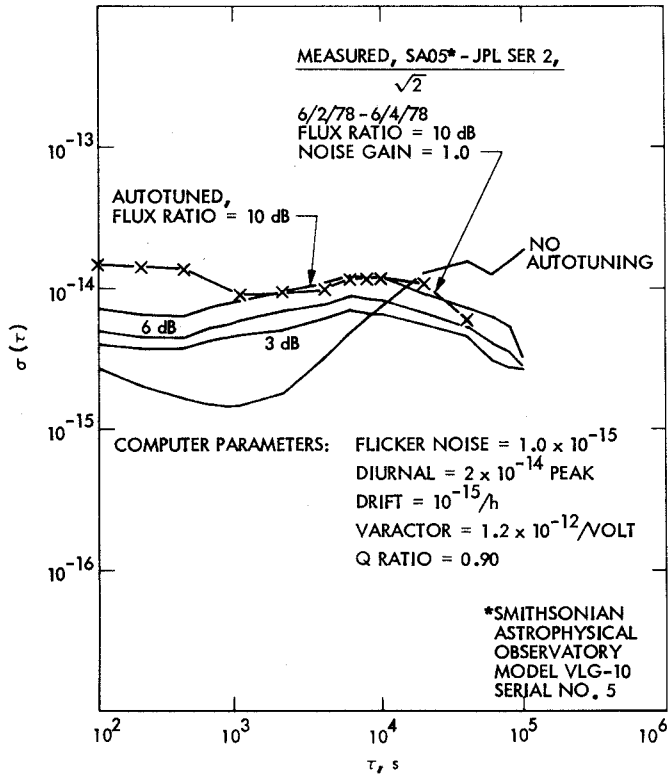


Fig. 9. Computer autotuner simulations, noise gain = 1.0 V/s, Q ratio = 0.90

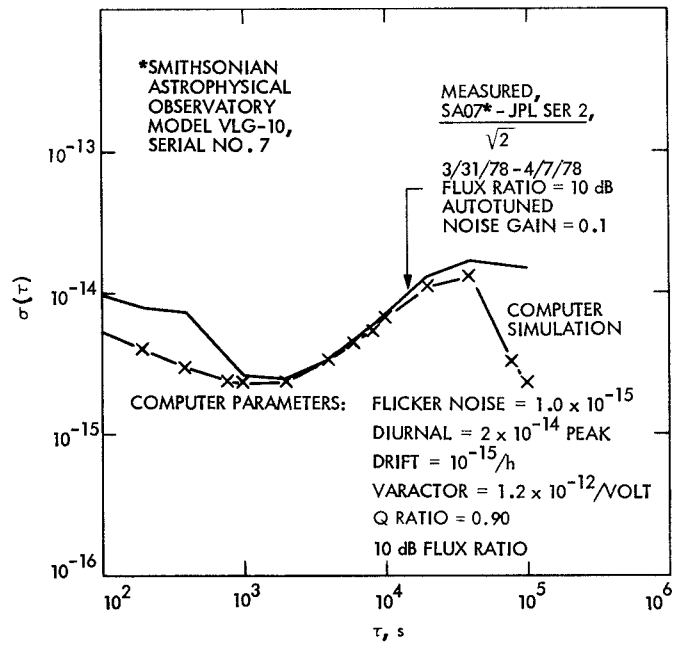


Fig. 10. Computer autotuner simulation, noise gain = 0.1 V/s, Q ratio = 0.90

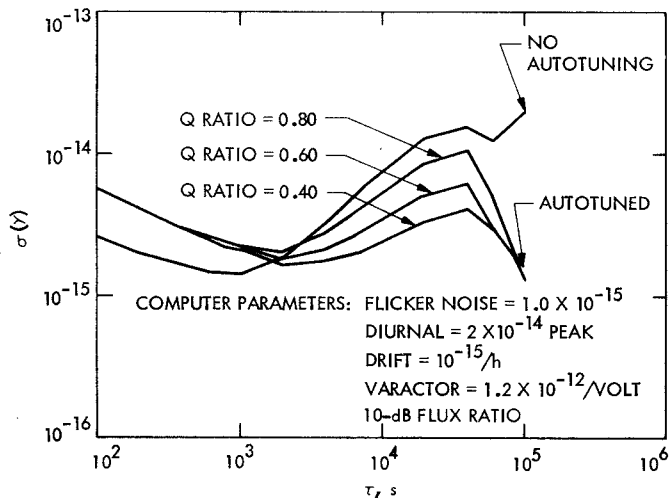


Fig. 11. Computer autotuner simulations, effect of Q ratio

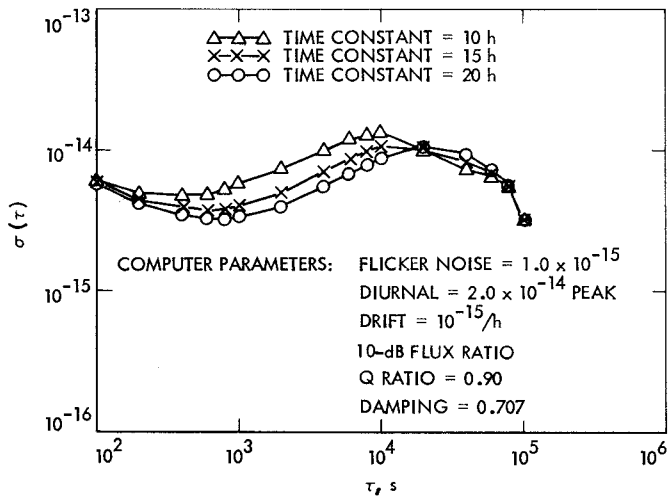


Fig. 13. Second-order autotuner simulations, effect of loop time constant

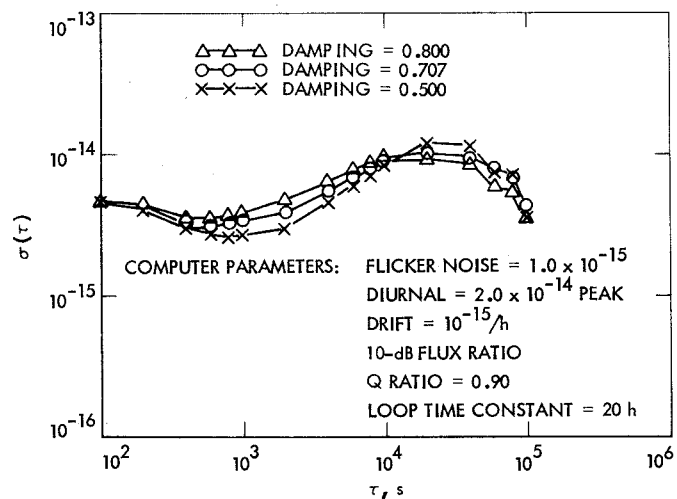


Fig. 12. Second-order autotuner simulations, effect of loop damping

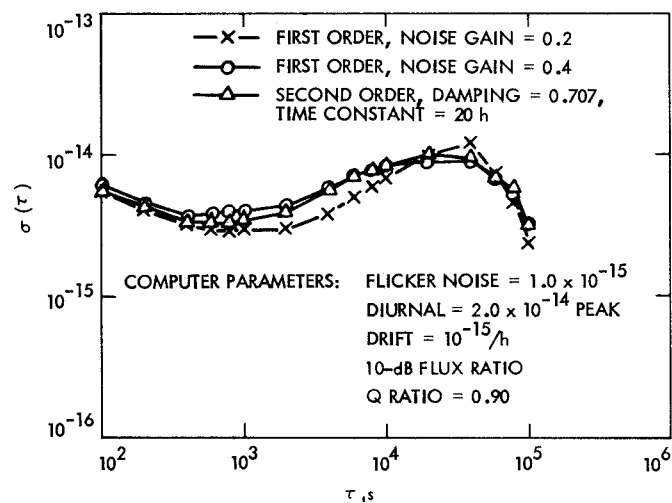


Fig. 14. Comparison of first- and second-order autotuner loops